

RACE AND CALCULATIONS OF THREE DIMENSIONAL DISTRIBUTED CAVITY PHASE SHIFTS

*Ruoxin Li and Kurt Gibble, The Pennsylvania State University,
State College, PA*

1. ABSTRACT

The design for RACE, a Rb-clock flight experiment for the ISS, is described. The cold collision shift and multiple launching (*juggling*) have important implications for the design and the resulting clock accuracy and stability. We present and discuss the double clock design for RACE. This design reduces the noise contributions of the local oscillator and simplifies and enhances an accuracy evaluation of the clock.

As we try to push beyond the current accuracies of clocks, new systematic errors become important. The best fountain clocks are using cylindrical TE₀₁₁ microwave cavities. We recently pointed out that many atoms pass through a node of the standing wave microwave field in these cavities. Previous studies have shown potentially large frequency shifts for atoms passing through nodes in a TE₀₁₃ cavity. The shift occurs because there is a small traveling wave component due to the absorption of the copper cavity walls. The small traveling wave component leads to position dependent phase shifts. To study these effects, we perform Finite Element calculations. Three-dimensional Finite Element calculations require significant computer resources. Here we show that the cylindrical boundary condition can be Fourier decomposed to a short series of two-dimensional problems. This dramatically reduces the time and memory required and we obtain (3D) phase distributions for a variety of cavities. With these results, we will be able to analyze this frequency shift in fountain and future space clocks.

2. INTRODUCTION

The principal advantage of microgravity for atomic clocks is interrogation times longer than 1 s. With a 10 s interrogation time, a clock has a 50 mHz linewidth suggesting that accuracies may approach 10⁻¹⁷. However, to achieve greater accuracy within the same averaging time, greater stability is needed. RACE is based on Rb to avoid the large cold collision shift of Cs.[1,2] This may allow simultaneously high short-term stability and accuracy. We have three primary goals: (1) Demonstrate new clock techniques for laser-cooled atoms to enable frequency comparisons with accuracies of 1 part in 10¹⁷. (2) Significantly improve the classic clock tests of general relativity. (3) Distribute accurate time and frequency from the ISS. We review the design constraints and discuss the double clock design for RACE.

Current atomic fountain clocks have inaccuracies near 10⁻¹⁵. Losses in the microwave cavities lead to small traveling wave components that deliver the power from the cavity feed to the walls of the cavity.[3] The small traveling wave components produce a microradian distribution of phases throughout the cavities, and therefore distributed cavity phase shifts need to be considered. LeMonde *et al.* have shown that there are large phase shifts in multi-Rabi TE₀₁₃ cavities due to the traveling wave

component near the nodes of the standing wave.[4] These phase shifts produce large frequency shifts of order 10^{-13} for $\pi/2$ excitation and 10^{-11} for $3\pi/2$ pulses.

Using finite element analysis to study the TE_{011} microwave cavity, we found that there are nodes through which the atoms pass.[5] The nodes occur in the cut-off waveguide sections used to prevent microwave leakage from the cavity. By symmetry, the lowest coupled mode is the TE_{01} . The longitudinal magnetic field in the TE_{01} waveguide mode reverses between the center and the copper boundary. Therefore, there must be a node in the time-dependent field the atoms experience as they pass through the cavity with trajectories near the waveguide wall. Hence one might expect large phase shifts due to traveling wave components for these atoms.

Three-dimensional Finite Element calculations require significant computer resources. Here we show that the boundary condition on the cylindrical cavity walls can be Fourier decomposed in a basis of $\cos(n\phi)$. [6] This reduces the 3D problem to a Fourier series of 2D problems. Because the atoms pass through the center of the cavity and because the wave equation solutions are proportional to ρ^n , only 3 to 4 terms in the series are required to accurately calculate the 3D phase of the microwave field. This reduces hours of calculations to seconds. With these results, we can analyze the frequency shifts in earth and space clocks due to distributed cavity frequency shifts.

3. DESIGN OF JUGGLING CLOCKS AND RACE

To achieve the potential accuracy of laser-cooled microgravity clocks with reasonable integration times, atoms must be multiply launched (juggled). Juggling imposes several constraints on the design of a microgravity clock. Shutters are needed to block the light scattered from trapping, state preparation, and detection from the interrogation region. In Figure 1, we show a design for a juggling

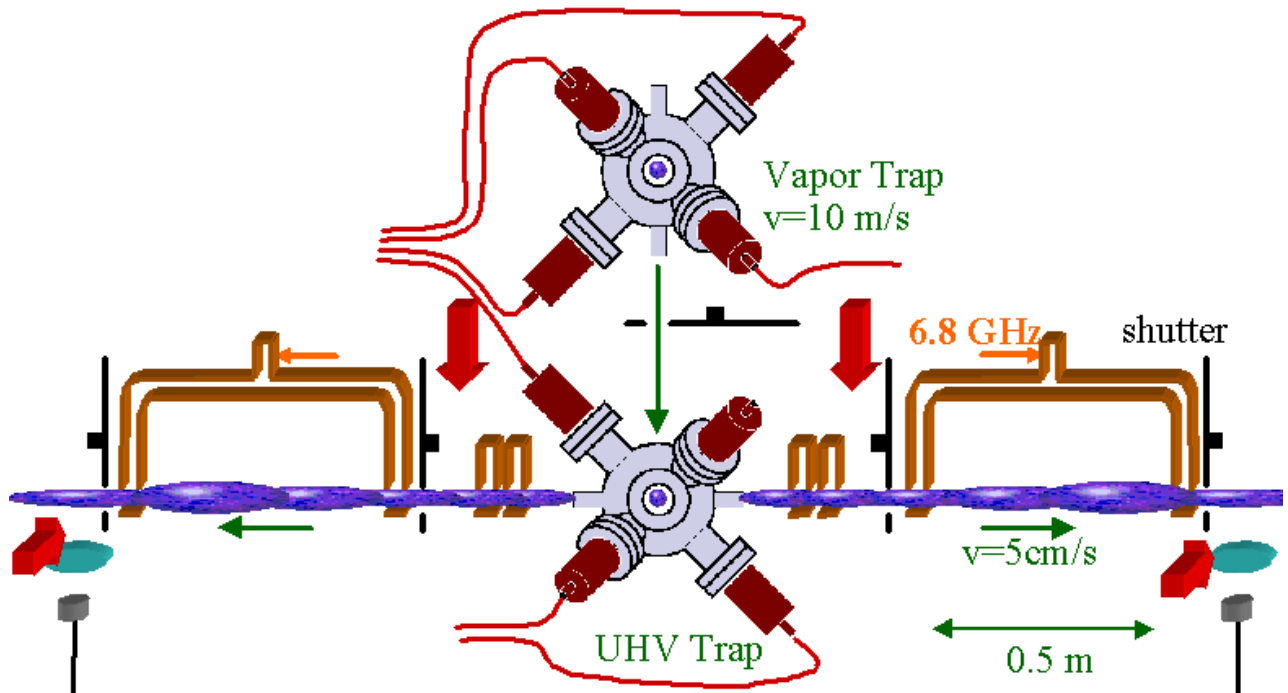


Figure 1. Schematic for juggling microgravity Rb clock RACE. The double MOT launches atoms at high speed from the (upper) vapor trap to the (lower) UHV trap so that the shutter between the traps can be nearly always closed. The shutters between the UHV trap and the cavities are nearly always open except during the ≈ 5 ms that the light for the UHV trap is turned on. The atoms are alternately launched left or right to go through one clock cavity or the other.

microgravity clock that has a pair of shutters surrounding the Ramsey cavity. This is a design for our Rb microgravity clock, RACE. First we discuss the laser trapping and cooling techniques and then the advantages of having 2 clock cavities.

The double-MOT[7,8] allows a high throughput of cold atoms and therefore a high short-term stability. The high throughput is possible because the double-MOT can rapidly capture many cold atoms and then efficiently launch them through the Ramsey cavity. The “upper” vapor cell trap in Fig. 1 essentially continuously traps atoms and then launches them at 5-10 m/s to the UHV trap “below.” Because of the high launch velocity from the vapor cell trap, the atoms pass quickly through the shutter separating the 2 traps. This implies that the shutter only needs to open for the short time that the ball of atoms flies through, and only during that time must the lasers for the vapor-cell trap be extinguished to prevent light from entering the interrogation region.

The real advantage of the double-MOT design comes from the fact that the UHV trap can capture and launch a ball of atoms in as little as 5 ms. This implies that the shutter separating the UHV trap and interrogation region only has to close for 5 ms for each launch and therefore is nearly always open. This allows a high throughput since, if the shutter is ~10 cm from the center of the UHV trap, the ball of atoms will have expanded considerably before reaching the shutter. For our juggling Cs experiment,[8] it was crucial to reduce the trapping and cooling time of the UHV trap be able to study collisions at low energies (corresponding to juggling rates as high as 140 s^{-1}).

One also has to worry about the effect of the trapping light on the previously launched ball of atoms from the 2nd trap. Again, this was a crucial step in our Cs juggling experiment. By “hiding” the ball in the lower hyperfine state immediately after the launch, and by carefully controlling the low intensity repumping light to the 2nd trap, we can capture and launch balls of atoms almost on top of one another.[8]

The RACE schematic in Fig. 1 shows 2 clock cavities. After atoms are collected in the lower laser trap, they are launched either through one cavity or the other. Having 2 cavities is important for a number of reasons. One advantage is that it greatly reduces the requirements for the local oscillator. Few oscillators can perform at the $\sigma_y(\tau) = 3 \times 10^{-15} \tau^{-1/2}$ level and there would be significant work required to develop their flight worthiness. The essential problem with only a single cavity results from the fact that the microwave frequency fed to the cavity must be changed from one side of the transition to the other. During the switch-over, all of the atoms must be cleared from the cavity and this means the oscillator is not tracked for about 10 s when $T = 10 \text{ s}$. With 2 cavities, we can do the switch-over for one cavity while still monitoring the oscillator with the other cavity and therefore the stability of the clock is so affected by the local oscillator instability.

Vibrations on the ISS in the direction of the launch velocity cause a noise in the interrogation time. With 2 cavities, the 2 detected signals will behave oppositely so that the effects of vibrations can be identified, correlated with an accelerometer, and removed. Furthermore, one of the largest systematic errors is the AC Stark shift due to blackbody radiation at 300K. A measurement of the red shift and time dilation with frequency inaccuracies of 10^{-17} demands absolute knowledge of the average temperature in the clock cavity at the 0.01K level. Having 2 cavities will allow a critical check on our accuracy evaluation. In addition, having 2 cavities gives important redundancy. For example, if a shutter fails in the closed position, we will still be able to achieve mission success goals (although requiring longer averaging times).

4. CALCULATIONS OF DISTRIBUTED CAVITY PHASE SHIFTS

Nearly all current primary fountain clocks use a cylindrical TE_{011} cavity to excite the atoms. In Figure 2, we show contours of the magnitude of the longitudinal magnetic field (H_z) in a TE_{011} cavity. Those atoms that pass near the wall of the waveguide when they enter or exit the cavity first experience a field that is reversed (π phase shift) relative to that at the center of the cavity.[5] Therefore, there must be nodes for atoms passing near the walls and, from [4], one could expect large phase errors for atoms passing through these regions. In fact, atoms going through nearly half of the area of the aperture on each pass see a field reversal and therefore a node in the field.

Losses in the cavities imply there is a small traveling wave component in addition to the large standing wave. The traveling wave component leads to phase gradients in the cavity.[3,9] Therefore, atoms passing through different regions, especially different regions on the upward versus downward passages, see a different effective phase of the microwave field. This can lead to a frequency shift of the clock known as the distributed cavity phase shift.[10] The distributed cavity phase shifts can be particularly large at nodes of the field as the traveling wave dominates at the nodes of the standing wave.

The traveling wave field, due to the losses, is not easy to calculate analytically – it mixes many modes. Khursheed, Vecchi, and DeMarchi used a finite element method to calculate the traveling wave field and the phase shifts for an infinitely long two-dimensional cylindrical cavity.[9] Extending the calculations to three dimensions requires vastly greater memory and computation time; the time required scales as $T_{2D}^{3/2}$. Here we show that the three dimensional problem can be expressed as a quickly converging series of two-dimensional problems. This shortens calculations requiring hours on current personal computers to seconds.

Following Khursheed, Vecchi, and DeMarchi, we can decompose the microwave field in the cavity into a standing wave H and a small traveling wave g .[9] Here, we are particularly interested in the z components (along the cylindrical axis) of these fields. H , g , and, by superposition, $H+g$ are solutions to Maxwell's equations. The boundary conditions for H_z are zero on the top and bottom endcaps and a zero normal derivative on the cylindrical walls of the cavity and the cut-off waveguide sections. For g_z , the boundary conditions on the top and bottom endcaps is

$$g_z = \frac{1+i}{\sqrt{2\sigma\mu\omega}} \nabla \times (\hat{n} \times H) \hat{z} \quad \text{and} \quad \text{the normal}$$

$$\text{derivative on the cylindrical walls is} \quad \frac{\partial g_z}{\partial n} = (1-i) \sqrt{\frac{\omega\epsilon_0}{2\sigma}} k H_z \quad \text{where } \omega = 2\pi \times 9.192 \text{ GHz, } \epsilon_0$$

is the vacuum permittivity, μ is the vacuum permeability, σ is the conductivity (of copper), and k is the microwave wave vector. These cavities are

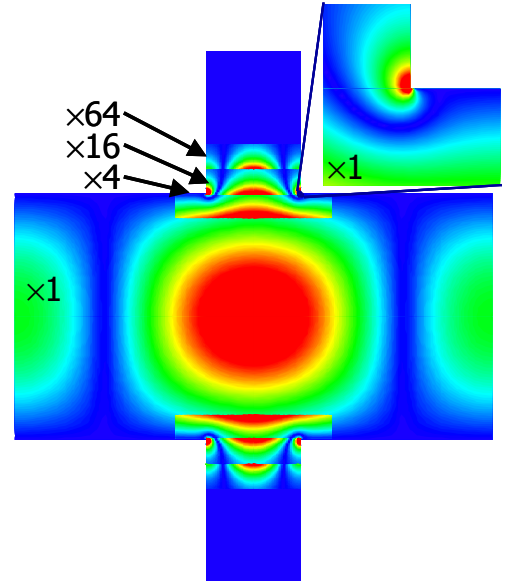


Figure 2. Contours of the magnitude of the longitudinal magnetic field, H_z , in a cylindrical TE_{011} cavity. The cavity height 26.075 mm, the radius is 25.5 mm, and the apertures have a 1cm diameter. The field near and in the cut-off waveguide sections are magnified by 4, 16, and 64 times. The line of field nodes (blue) in the below cut-off waveguide sections extend into the cavity and can be clearly seen in the magnified section. The field strength, where the cut-off section meets the cavity (red), is comparable to the peak field in the (red) center of the cavity (with π phase shift).

fed by one, two, or four small holes distributed around the cavity's midsection. At the feed, the boundary condition for $\partial g_z / \partial n$ is given by balancing the power fed into the cavity against the losses in the walls. An example of the boundary condition at the midsection for a single cavity feed is shown in Figure 3.

The boundary condition in Figure 3 can be expressed as a Fourier series $\sum_n A_n(z) \cos(n\phi)$ and we can write $g_z(\rho, \phi, z) = \sum_n g_n(\rho, z) \cos(n\phi)$. [6] Then, g_n satisfies the two-dimensional wave equation

$$\left[\frac{1}{\rho} \frac{\partial}{\partial \rho} \left(\rho \frac{\partial}{\partial \rho} \right) - \frac{n^2}{\rho^2} + \frac{\partial^2}{\partial z^2} + k^2 \right] g_n(\rho, z) = 0 \quad (1).$$

Because the feed is very small, to preserve a cavity $Q > 10,000$, many n are required to get the full solution of g_z ; as the feed approaches a delta function, $n \rightarrow \infty$ is required. However, for $\rho \rightarrow 0$, the

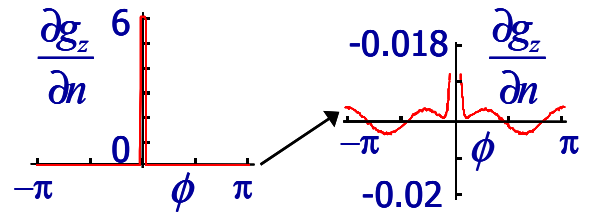


Figure 3. Boundary condition for the traveling wave field g_z at the midsection of a cavity with a single feed. Power is supplied at $\phi \approx 0$ and there are small losses at all other ϕ . The 1% variation of the losses is due to the proximity of the TE_{311} modes and could be neglected.

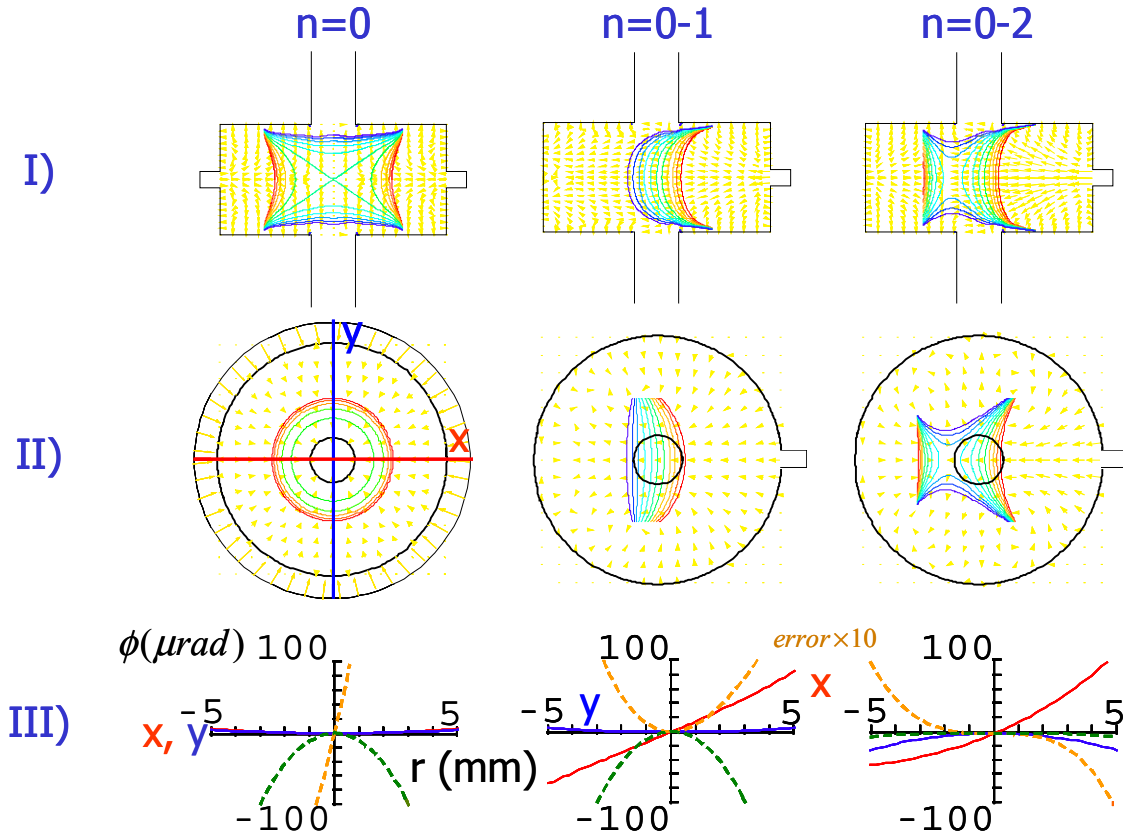


Figure 4a. Phase contours of $H_z + g_z$ and the Poynting vector in I) the x - z plane and II) the $z=0$ plane. Phase contours are $25 \mu\text{rad}$ steps. Each is shown for 1, 2, & 3 terms in the azimuthal expansion. III) The phase (solid line) and errors (dashed lines) plotted versus x and y for $z=0$. The error is the difference between the phase for N terms versus that for 65 terms. For 3 terms ($n=0-2$), the maximum phase error in the central region is $\approx 10\%$.

asymptotic solution to Eq. 1 is ρ^n . Since the atoms pass through the center of the cavity, g_n , for large n , has a negligible effect and, as we show next, only $n \leq 2-3$ is required.

We Solve Eq. 1 on a triangular lattice for the cavity in Figure 2 for a variety of cavity feeds. For a single cavity feed, we choose the feed to be on the positive x -axis. The solution is symmetric about the x - y plane. (The solution is also symmetric about the x - z plane and therefore g_z is an expansion in $\cos(n\phi)$.) We therefore mesh $\rho, z \geq 0$ with 3,200 to 50,000 triangles and solve for g_n with $n=0-64$. [11]

In Figures 4a and 4b, we show the phase contours and Poynting vectors from a sum of g_n for $n=0-N$ for $N=0-4$ & 64. The $n=0$ term exactly describes a cavity that is fed azimuthally symmetrically at the midsection. Therefore, this term has very small phase gradients and the Poynting vectors show power flowing in at the midsection and flowing to all the other surfaces. For the $n=1$ midsection, power is supplied for positive x and, for negative x , power is removed to nearly balance that supplied by $n=0$. Higher n further distributes the power in the plane to construct the small feed. Due to the proximity of the TE_{311} resonance, the $n=3$ term has a noticeable effect on the power flow in the cavity. The series converges very rapidly; for 3 terms, the phase error near the center of the cavity is $\approx 10\%$ and for 4 terms it is less than 1%. The rapid convergence shows that the atoms are insensitive to localized cavity losses at surfaces far from the atoms' trajectories – it is only the average absorbed power over $\phi \approx \pi/4$ that affects the phase of the microwave field seen by the atoms. Irregularities in the cut-off waveguide sections, especially where the field is large near the junction of the cut-off section and the cavity, may have important effects.

Cavities with two and four feeds are commonly used. [12] These avoid the large flow of power across a cavity with a single feed that leads to the large phase gradient along the x axis shown in Figs. 4. In Fig. 5, we show calculations for two and four feeds. For two (four) feeds, g_z is a sum over g_n for

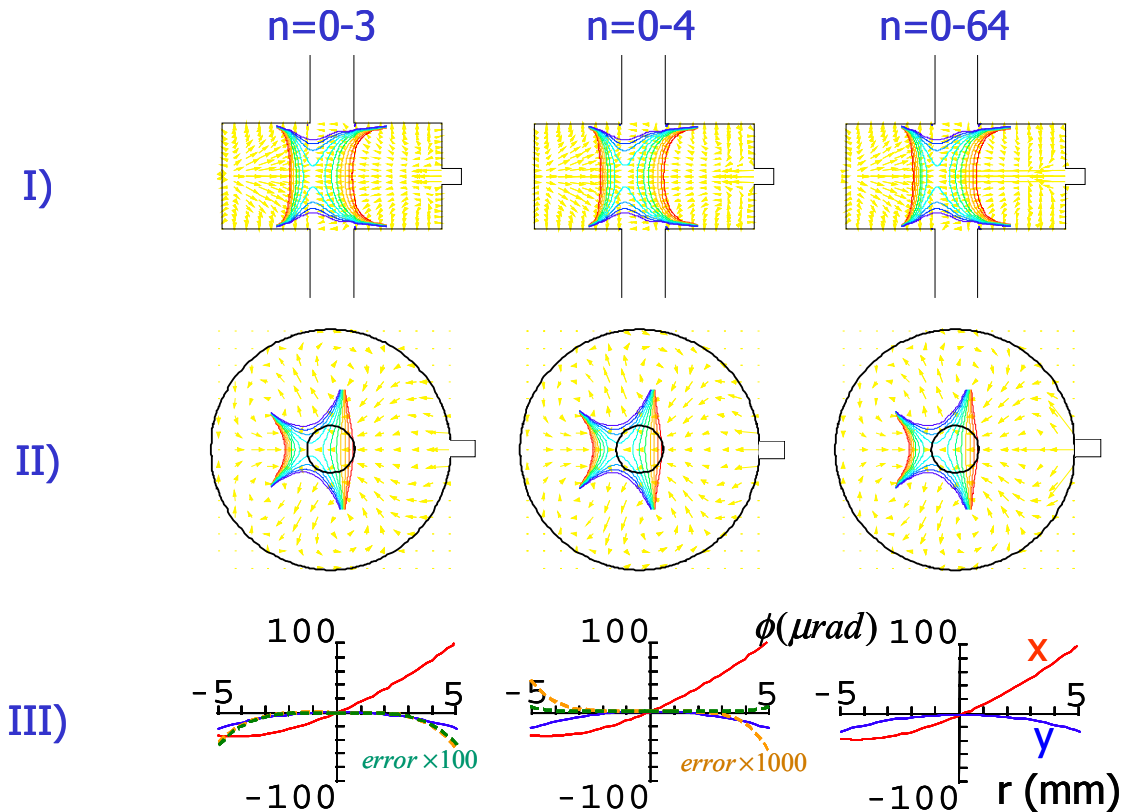


Figure 4b. The same quantities in Fig. 4a for 4, 5, and 65 terms of the azimuthal expansion. For 4 terms, the error is less than 1% or $1\mu\text{rad}$.

$n=0,2,4,6, \dots$
 $(0,4,8,12,\dots)$. These show significantly smaller phase gradients than a cavity with a single feed.

Armed with the three dimensional phase in the cavity, the atomic responses to the microwave field can be calculated. The dramatically faster computation of a series of 2D calculations will facilitate the optimization of cavities for atomic clocks. We are currently analyzing the effects of the large phase shifts near the standing wave nodes. This is important for the currently operating atomic clocks. For future clocks, it is not difficult to eliminate the nodes. One cavity design that eliminates this potential error is shown in Figure 6.[5]

A larger diameter section of cut-off waveguide is used. In this large diameter section the nodes are not sampled by the atoms and the field decays to a sufficiently small level. Then the smaller diameter waveguide section, which sets the cavity aperture, follows to insure a sufficiently small microwave leakage.

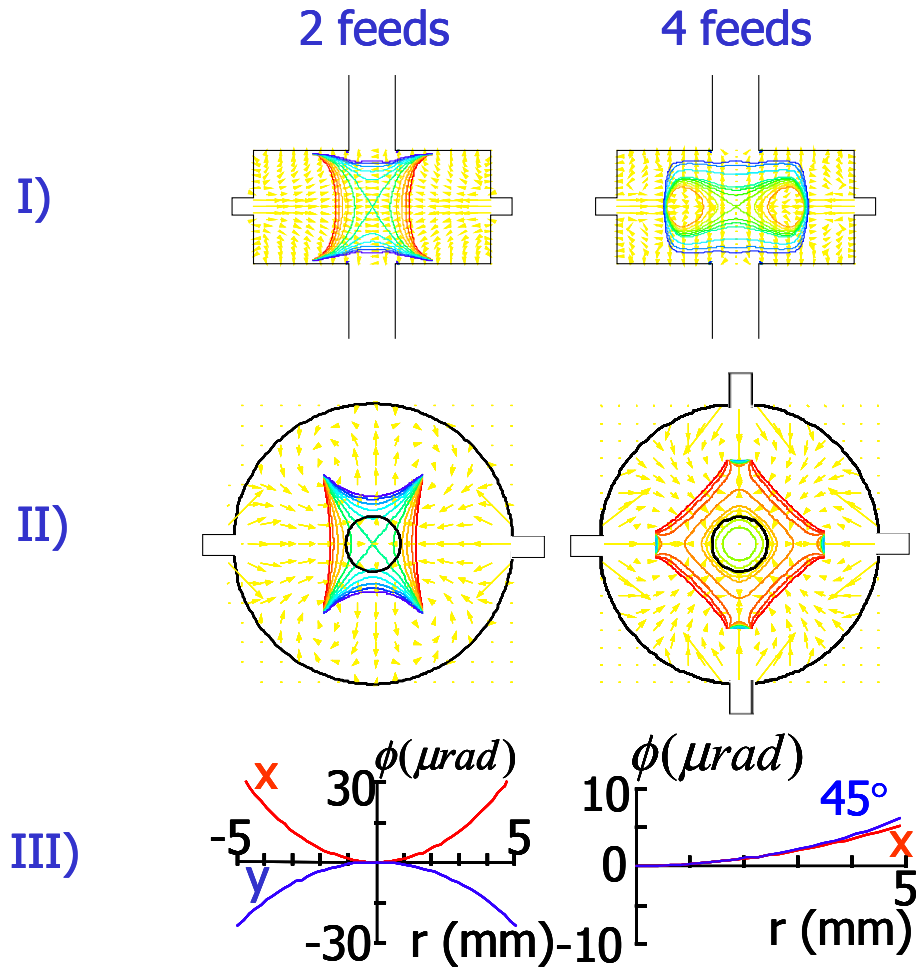


Figure 5. Phase contours of H_z+g_z and the Poynting vector for cavities fed by 2 and 4 ports in I) the x-z plane and II) the z=0 plane. Phase contours are 25 μrad steps. III) The phase for $z=0$ plotted versus x and y for the 2 feeds and versus x and along $x=y$ for 4 feeds. Both show smaller phase gradients than a cavity with a single feed.

5. CONCLUSIONS

To achieve the potential accuracy of laser-cooled microgravity clocks with reasonable integration times, atoms must be multiply launched (juggled). The short-term stability is proportional to the launch rate and this in turn implies that high accuracy and stability favor long interrogation regions. Laser-cooled microgravity clocks can achieve short-term stabilities approaching $\sigma_y(\tau) = 3 \times 10^{-15} \tau^{-1/2}$. At this stability, the largest uncertainty in a Cs microgravity clock is likely to be the cold collision frequency shift. By using ^{87}Rb , the collision shift is 50 times smaller allowing an accuracy of 10^{-17} . We describe the design of our Rb microgravity clock which uses a double-MOT and 2 cavities. This simplifies the trapping and shutter design while maintaining a high throughput of cold atoms, minimizes

the local oscillator requirements, eliminates errors due to vibrations, and provides failure and accuracy redundancy.

The commonly used TE_{011} cylindrical cavities have nodes in the field regions sampled by the atoms. Near the nodes there may be significant phase shifts, especially near the wall of the cutoff waveguide apertures, and this effect may interact with other errors to produce a tilt sensitivity of fountain clocks.

We have shown that the 3D distribution of the phase of the microwave field in a cavity can be expressed as a 2D azimuthal expansion. This dramatically reduces the needed computing time (and memory). These gains will facilitate improvements in microwave cavity designs for earth and space-based atomic clocks.

6. ACKNOWLEDGEMENTS

We acknowledge financial support from the NASA Microgravity program and Penn State University.

7. REFERENCES

- [1] C. Fertig and K. Gibble, Phys. Rev. Lett. **85**, 1622 (2000).
- [2] K. Gibble and S. Chu, Phys. Rev. Lett. **70**, 1771 (1993).
- [3] G. Vecchi and A. De Marchi, IEEE Trans. Instr. Meas. **42**, 434 (1993).
- [4] P. Lemonde, G. Santarelli, Ph. Laurent, F. Pereira, A. Clairon, and Ch. Salomon, Proceeding of the Freq. Contr. Symp., p. 110, (1998)
- [5] C. Fertig, R. Li, J. I. Rees, and K. Gibble, Proc. 2002 IEEE Freq. Contr. Symp., 469 (2002).
- [6] C.L. Britt, IEEE Trans. Antenna and Propagat. **37**, 1181 (1989) ; Y. Chen, R. Mittra, P. Harms, IEEE Trans. Microwave Theory and Tech. **44**, 832 (1996).
- [7] K. Gibble, S. Chang, and R. Legere, Phys. Rev. Lett. **75**, 2666 (1995).
- [8] R. Legere and K. Gibble, Phys. Rev. Lett. **81**, 5780 (1998).
- [9] Khursheed, Vecchi, & DeMarchi, IEEE Tran. UFFC **43**, 201, 1996.
- [10] A. Bauch, T. Heindorff, and R. Schroeder, IEEE Trans. Instrum. Meas. **34**, 136 (1985).
- [11] For $n=0$, the wave equation has a scalar solution for g_z that does not satisfy Maxwell's equations. For $n=0$, we solve instead for the $\hat{\phi}$ component of the electric field and obtain the magnetic field from it.
- [12] See for example A. Clairon, S. Ghezli, G. Santarelli, Ph. Laurent, S. N. Lea, M. Bahoura, E. Simon, S. Weyers, and K. Szymaniec, Proc. Fifth Symp. Freq. Standard and Metrol., 49 (1995); C. R. Ekstrom, E.A. Burt, T.B. Swanson, Proc. 2001 IEEE Freq. Contr. Symp., 53 (2001); S.R. Jefferts, R.E. Drullinger, A. DeMarchi, Proc. 1998 IEEE Freq. Contr. Symp., 6 (1998); S. Weyers, U. Hubner, R. Schroder, C. Tamm, A. Bauch, Digest 2000 Conf. Prec. Electromagnetic Meas., 632 (2000); F. Levi, L. Lorini, D. Calonico, A. Godone, IEEE Trans. Instr. Meas., **52**, 267 (2003).

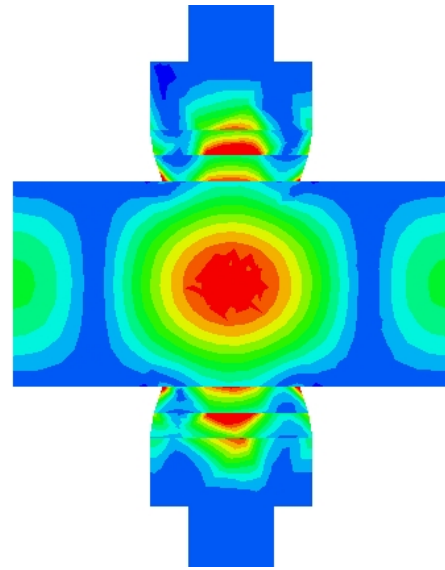


Figure 6. Contours of the magnitude of H_z in a cylindrical TE_{011} cavity with cutoff waveguide sections of different diameter. The larger diameter waveguide sections have nodal lines outside of the region through which atoms pass. In the smaller diameter section, H_z , while it has nodes, can be sufficiently small.